*Bangladesh Journal of Physics, Vol. **28**, Issue 1, pp. 25-37, June 2021*

STEP ANNEALING EFFECT ON CRYSTALLIZATION KINETICS AND ACTIVATION ENERGY OF $Fe_{30}Ni_{50}B_{20}$ AMORPHOUS METALLIC GLASS RIBBON

S. YASMIN TISA[1], S. D. NATH[1], S. K. SHIL[1], S. I. LIBA[2], M. N. I. KHAN[2] AND S. S. SIKDER[1*]

[1]*Department of Physics, Khulna University of Engineering & Technology, Khulna, Bangladesh*
[2]*Materials Science Division, Atomic Energy Centre, Dhaka, Bangladesh*

[*]*Corresponding author e-mail: sssikder@phy.kuet.ac.bd*

Received on 26.03.2021, Revised received on 14.05.2021, Accepted for publication on 11.06.2021

DOI: https://doi.org/10.3126/bjphy.v28i1.78586

ABSTRACT

The metallic glass with composition $Fe_{30}Ni_{50}B_{20}$ in the form of ribbon has been prepared by rapid solidification using a melt spinning technique at a wheel speed of 25 m/s in Ar atmosphere. This ribbon has been studied based on different annealed effects in associated structural kinetics and activation energy using Differential Thermal Analysis (DTA) and XRD analysis. The impact of annealing in the range of 200 °C to 400 °C with two steps constant annealing time has been compared with its amorphous states by DTA and XRD techniques. From DTA experiments, one exothermic peak, α-Fe(Ni) is found which is responsible for the softness of metallic glass ribbon at as-cast state and with increasing annealing temperature, the peak temperature of α-Fe(Ni) phase shifts toward higher temperature which agrees well with the XRD patterns. The activation energy of the annealed and as-cast ribbon samples is obtained within the range of 3.30 to 3.91 eV. In the optimized annealing temperature above 350 °C, the grain size obtained from XRD patterns in the range between 8-29 nm and the lattice parameter shifts to higher values with increasing annealing temperature as well as with constant holding time. The desired initial permeability below the glass transition temperature of the metallic glass ribbon depends on the best choices of parameters and its annealing effects with constant annealing time.

Keywords: *Amorphous ribbon, DTA, Crystallization, Activation energy, XRD, Permeability*.

1. INTRODUCTION

Typically, limited choices of Fe-Ni rich metallic glass ribbons are realized fluctuating positive and negative exchange interaction lead to complex non collinear spin glass structures [1]. In broader sense, desire of large magnetic inductions especially for high temperature applications of soft magnetic properties requires intrinsic or extrinsic properties through optimization crystallization kinetics with varying annealing temperature and annealing time. The effects of metallic ribbon compositions greatly hamper crystallization and show quite different behavior, leads to severe degradation of soft magnetic properties compare to original amorphous state [2]. Glass transition temperature interferes with the Curie temperature which restricts magnetic properties in the amorphous state. The dynamic soft magnetic properties with various composition changes of the novel material represent a new family of excellent soft magnetic core materials and their potential applications stimulated an enormous research activity [3-6]. The macroscopic average structural kinetics of metallic ribbon properties in magnetic spin glass

in atomic scale is perturbed by structural disorder [7, 8]. First DTA peak corresponds to precipitation of ordered bcc α-Fe(Ni) solid solution embedded in the amorphous phase transition and secondary peak corresponds to the boride phase which has an effect on the activation energy of crystallization process [7, 9]. Soft magnetic metallic glass alloy shows great interest because annealing effect of dynamic properties can disclose its potential application in various electronic devices and transformers. Thermal stability of amorphous metallic glass ribbons with respect to their operational temperature can be used reliably in technological applications of those metallic ribbons [10, 11]

In this research, an amorphous metallic ribbon with nominal composition $Fe_{30}Ni_{50}B_{20}$ has been prepared and the energy barriers to nucleation and growth of crystalline phase with different thermal treatments such as annealing temperature as well as annealing time have been studied. As a demonstration, the magnetic permeability as a function of frequency of the ribbon in the as-cast state and in different annealed states has also been investigated. It is expected that the noticeable change in microscopic grain size due to various annealing techniques would improve the magnetic property of the as prepared metallic ribbon.

2. EXPERIMENTAL DETAILS

Amorphous metallic ribbon with composition $Fe_{30}Ni_{50}B_{20}$ has been prepared in an arc furnace on a water-cooled copper hearth under an atmosphere of pure Ar. The high purity constituent elements are Fe (99.9%), Ni (99.9%) and B (99.9%) and obtained from Alfa Aesar. Melt spinning is a widely used production method for rapidly solidifying materials as well as preparing amorphous metallic ribbons [12, 13]. In order to prepare the ribbons form of $Fe_{30}Ni_{50}B_{20}$ alloy, melt spinning facilities was used at the Centre for Materials Science, National University of Hanoi, Vietnam. DTA measurements have been done using a thermogravimetric Analyzer TG/DTA/DSC (HITACHI Instruments TA7000 Series) from heating rates 10 to 60° in the step of 10°. The metallic ribbons are annealed at 200, 225, 250, 275, 300, 350 and 400 °C for constant holding time of one hour and for 30 minutes using MTI Corporation built 1700X-S High Temperature Muffle furnace. Following the annealing, the work pieces were left in the oven in order to have a controlled cooling process.

Crystalline phases of the metallic ribbon alloy were determined using a X'Pert Pro X-ray diffractometer with Cu-K_α radiation and a primary beam of 40 kV and 30mA. A 2θ scan was taken from 30˚ to 70˚ with a step size of 0.02˚ over 10 to 15 mg powder sample to obtain possible fundamental peaks where Ni filter was used to reduce Cu-K_α radiation.

To study the frequency dependent permeability, a section of the metallic ribbon is wound in the form of a toroid shape. A Wayne Kerr Impedance Analyzer (6500B) was used to examine the frequency dependent permeability of the toroid-shaped samples. The length of the metallic glass ribbon shaped sample is used as magnetic path length of toroidal coil sample and Cross-sectional area of this ribbon sample is used as the product of the thickness and width of the metallic ribbon.

3. RESULTS AND DISCUSSION

3.1 DTA analysis

The DTA patterns of $Fe_{30}Ni_{50}B_{20}$ metallic ribbon as-cast, annealed at 250 °C and 300 °C each for a constant annealing time 30 minutes are presented in Fig. 1 to Fig. 3 respectively. DTA traces of ribbon annealed at 200 °C, 250 °C and 300 °C each for constant holding time of one hour are presented in Fig. 4 to Fig. 6 respectively. All DTA traces were measured with heating rates 10 °C to 60 °C/minute at a step of 10 °C taken in a nitrogen atmosphere with continuous heating up to 800 °C at room temperature. In Fig. 1 to Fig. 6, all DTA results give two different crystallization events named glass transition temperature (T_g) and crystallization temperature (T_x) which are observed from the exothermic peaks respectively.

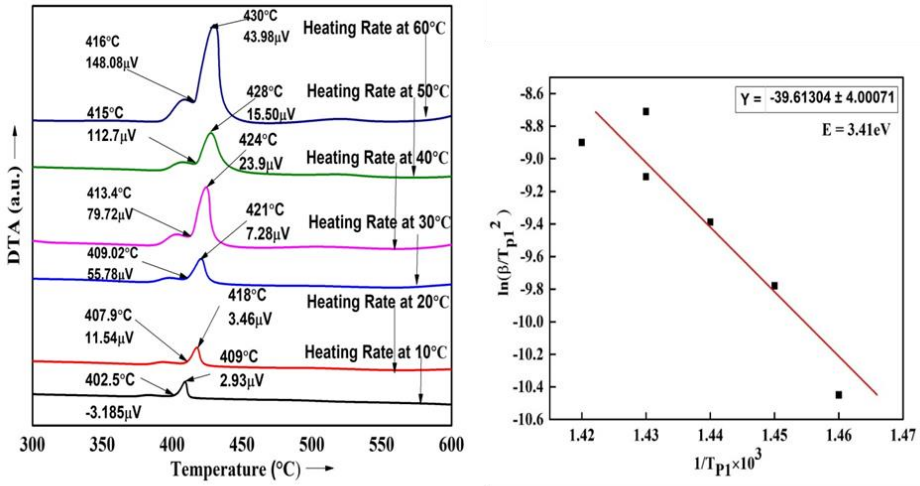

(a) (b)

Fig. 1 (a) DTA traces for heating rates 10 to 60 °C/minute and (b) Kissinger's plot to determine activation energy of as-cast $Fe_{30}Ni_{50}B_{20}$ metallic glass ribbon

From each of DTA traces T_g, T_x, crystallization peak position temperature (T_p) and their energy products are obvious and are indicated by given arrow for different heating rates. Here the need for ΔT_x lies in identifying the stability of the resultant metallic ribbon to understand the right temperature range for heat treatment and the right temperature range for thermodynamic viewpoint application. The structure of the ferromagnetic ribbon's prominent second phase T_x is composed of α-Fe(Ni), which is the product of secondary crystallization phase and is detrimental for soft magnetic properties. The T_x is moderate level in absence of boron content in nominal composition $Fe_{30}Ni_{50}B_{20}$ in order to obtain an optimum nanoscale structure at annealed samples. The composition of metallic amorphous glass ribbon not only affects primary but also T_x because time and temperature needed for constituent metallic and metalloid atoms to have long range order depend on their bond energies [14, 15].

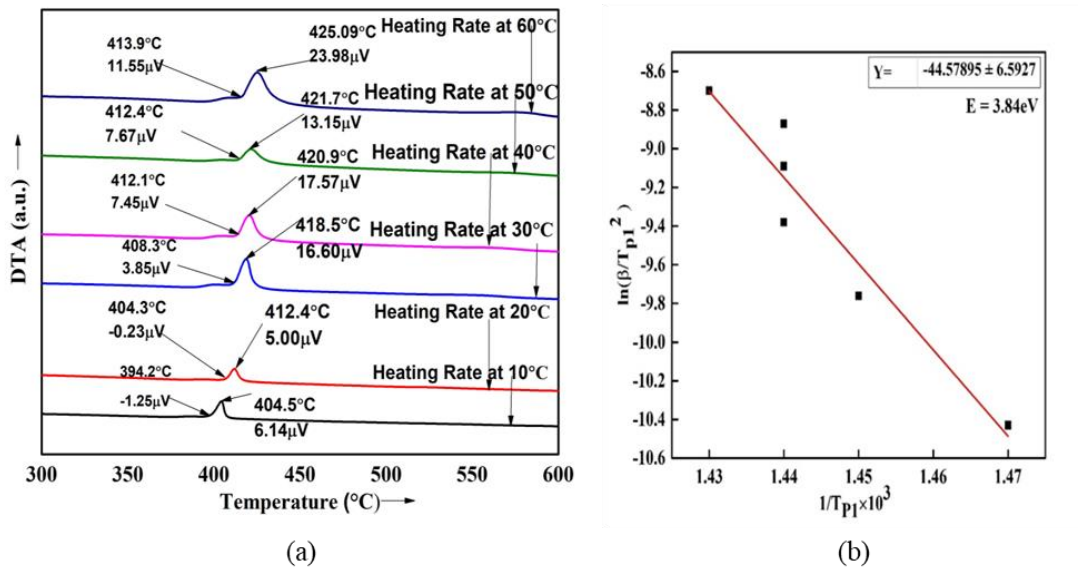

Fig. 2 (a) DTA traces for heating rates 10 to 60 °C/minute and (b) Kissinger's plot to determine activation energy of $Fe_{30}Ni_{50}B_{20}$ metallic glass ribbon annealed at 250 °C for holding time 30 minutes

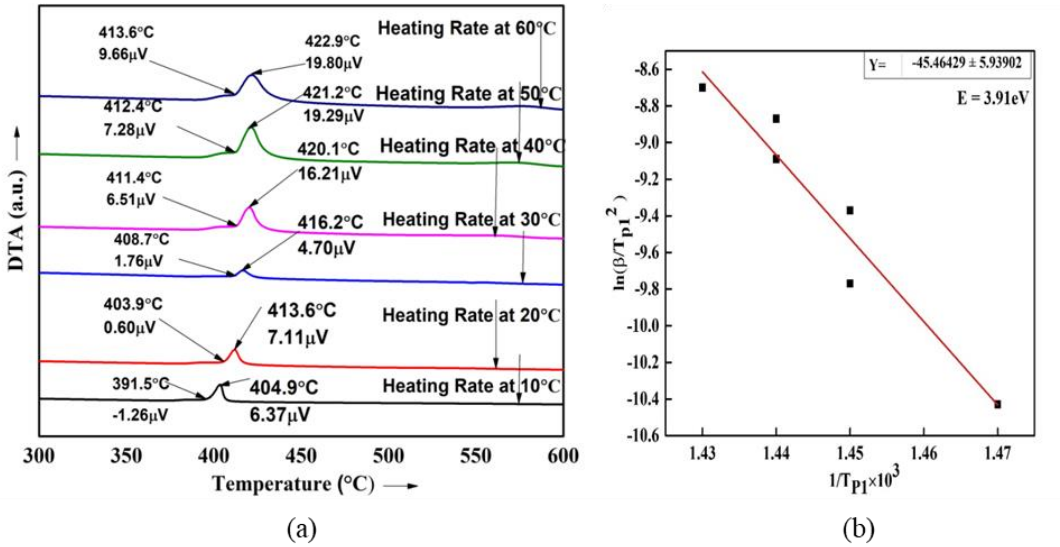

Fig. 3 (a) DTA traces for heating rates 10 to 60 °C/minute and (b) Kissinger's plot to determine activation energy of $Fe_{30}Ni_{50}B_{20}$ metallic glass ribbon annealed at 300 °C for holding time 30 minutes

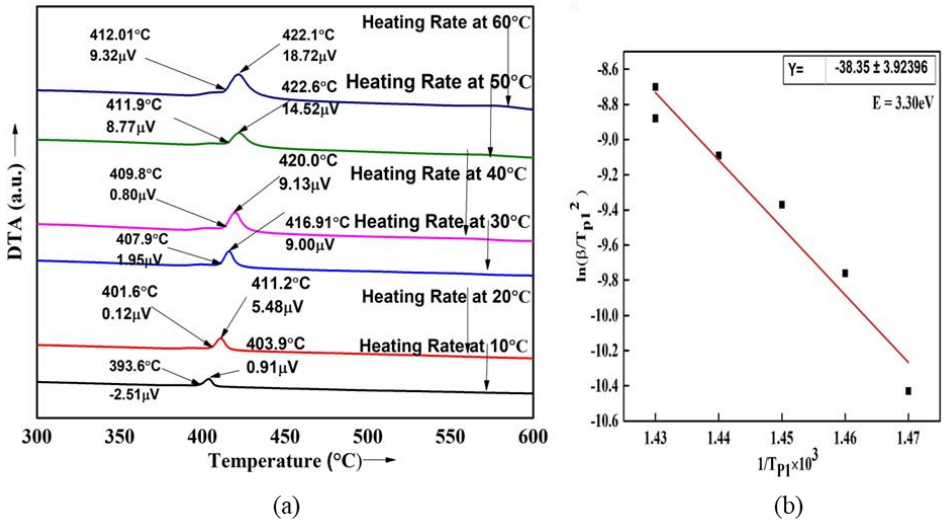

(a) (b)

Fig. 4 (a) DTA traces for heating rates 10 to 60 °C/minute and (b) Kissinger's plot to determine activation energy of $Fe_{30}Ni_{50}B_{20}$ metallic glass ribbon annealed at 200 °C for holding time 1 hour

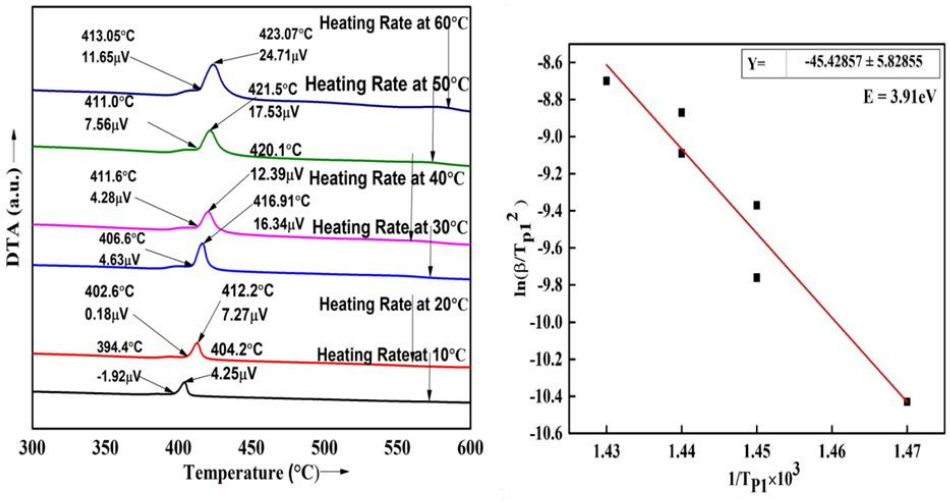

(a) (b)

Fig. 5 (a) DTA traces for heating rates 10 to 60 °C/minute and (b) Kissinger's plot to determine activation energy of $Fe_{30}Ni_{50}B_{20}$ metallic glass ribbon annealed at 250 °C for holding time 1 hour

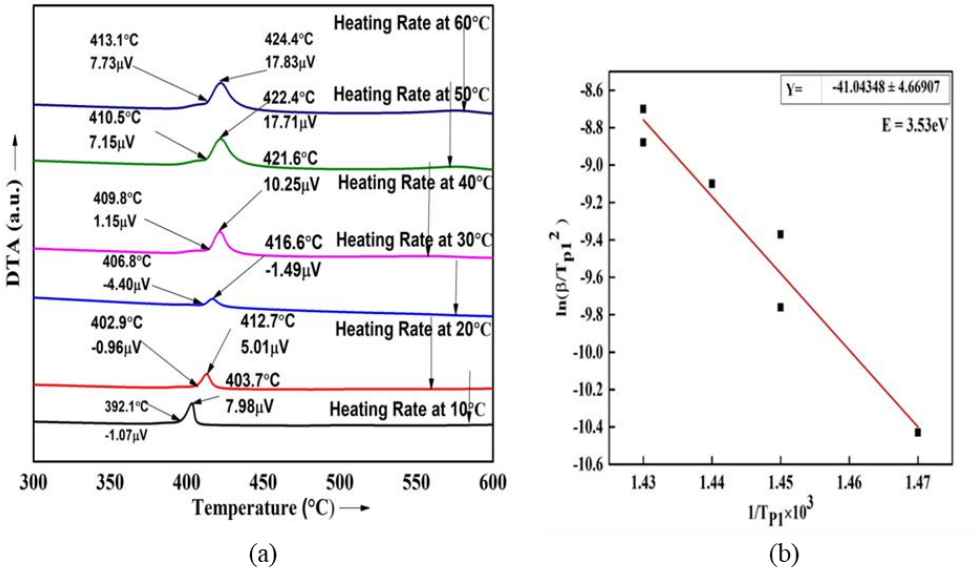

Fig. 6 DTA traces for heating rates 10 to 60 °C/minute and (b) Kissinger's plot to determine activation energy of $Fe_{30}Ni_{50}B_{20}$ metallic glass ribbon annealed at 300 °C for holding time 1 hour

The experimental data are collected from the DTA traces at constant heating rate 10 ºC/min for as-cast and short annealing time 30 minute from Fig. 1, Fig. 2, Fig. 3 and for higher annealing time 1 hour from the Fig. 4, Fig. 5 and are represented in Table 1 and Table 2 respectively. The results show that peak of corresponding to crystallization not significant changes but slightly decrease as-cast condition of present research alloy. The effect of annealing on crystallization peaks are corresponds to structural relaxation due to stress release initially formed by rapid solidification.

Table 1: The T_g, T_x, ΔT_x, T_p and energy products of crystallization states of $Fe_{30}Ni_{50}B_{20}$ for as-cast at constant heating rate 10 ºC/min and different annealed states for holding time 30 minutes

Annealing temperature (ºC)	T_g in °C	T_x in °C	ΔT_x in °C	T_p in °C	Starting energy products in T_g, μV-/mg	Finishing energy products in T_x, μV-S/mg	Peak position energy products in T_p, μV-S/mg
As-cast	400	415.09	15.09	409	-3.185	-5.37	2.93
250	394.2	415.2	21	404.5	-1.25	-2.35	6.14
300	391.5	414.5	23	404.9	-1.26	-2.22	6.36

The difference between the two crystallization positions, ΔT_x are almost unaffected by annealing condition and annealing time but just increased amorphous state. The crystallization peak T_p is completely diminished and displays diffused character means α-Fe(Ni) phase has already vanished for 350 ºC at constant holding time for various annealed samples. Energy products of T_g, T_x and T_p linearly increase with increasing annealing temperature for both short and higher annealing time in this amorphous sample. The kinetics of anisotropy depends on instantaneous reorientation of structural relaxation in terms of energy products increasing trends.

Table 2: The T_g, T_x, ΔT_x, T_p and energy products of crystallization states of $Fe_{30}Ni_{50}B_{20}$ for as-cast at constant heating rate 10 ºC/min and different annealed states for holding time 1 hour

Annealing temperature (ºC)	**T_g in °C**	**T_x in °C**	**ΔT_x in °C**	**T_p in °C**	**Starting energy products in T_g, µV-S/mg**	**Finishing energy products in T_x, µV-S/mg**	**Peak position energy products in, µV-S/mg**
As-cast	400	415.09	15.09	409	-3.185	-5.37	2.93
200	393.6	412.1	18.5	403.9	-2.51	-3.16	0.91
250	394.4	412.8	18.4	404.2	-1.92	-2.86	4.25

The activation energy of α-Fe(Ni) crystallization phase has been calculated using Kissinger equation [16] is given by

$$E = -KT_p ln\left(\frac{\beta}{T_p^2}\right)$$

Here β is heating rate, T_p is the crystallization peak temperature, E is activation energy and K is Boltzmann constant. Kissinger's plots are shown in Fig. 1 to Fig. 6 and the obtained data are listed in Table 3. It is seen that thermal crystallization activation energy increases with increasing annealing temperature for a lower annealing time of 30 minutes. The activation energy of transformation for viscous flow and other terms is omitted because significantly depends on the annealing temperature in that region of constant lower annealing time. The correlation between thermal stability ΔT_x and activation energy E using the time transformation to crystallization in the state of exothermic peak start rather than to the starting of T_g.

Table 3: The activation energy of $Fe_{30}Ni_{50}B_{20}$ amorphous ribbon for as-cast and various annealed states

Activation energy in eV						
Before annealing	**After annealing at**					
As-cast	200 ºC		250 ºC		300 ºC	
3.41	30 minutes	one hour	30 minutes	one hour	30 minutes	one hour
	.....	3.30	3.84	3.91	3.91	3.53

The activation energy of α-Fe(Ni) at initial annealing temperature 200 ºC decreases than as-cast amorphous phase after discontinues increasing trend with increasing annealing temperature for higher annealing time 1 hour as shown in Table 3. These discontinuous values of activation energy of the formation of crystallization phase, at temperature below the break single metastable crystalline phase form in the glassy state of this ribbon alloy. And also, energy product decreases while reversible relaxation effects utilize an activation energy being linearly related to the instantaneous value and an incubation time annealing implies that no suitable sized nuclei exist in as-quenched glass alloy.

3.2 XRD analysis

The XRD patterns of $Fe_{30}Ni_{50}B_{20}$ glass ribbon annealed at 250, 275, 300, 325, 350 and 400°C each for annealing time 1 hour and 30 minutes are presented in Fig. 7 and in Fig. 8 respectively. It is observed that above 325 °C clearly crystallization starts and with increasing annealing temperature the peaks show narrow and sharper with higher intensity which indicates α-Fe(Ni) grains are growing. The crystallization peak temperatures of DTA analysis for different heating rates are found around the 405 °C range, which shows good consistency with XRD spectra. The diffuse hallow below 350 °C annealed samples is amorphous in nature which means no crystallization occurs in the samples annealed below 350 °C.

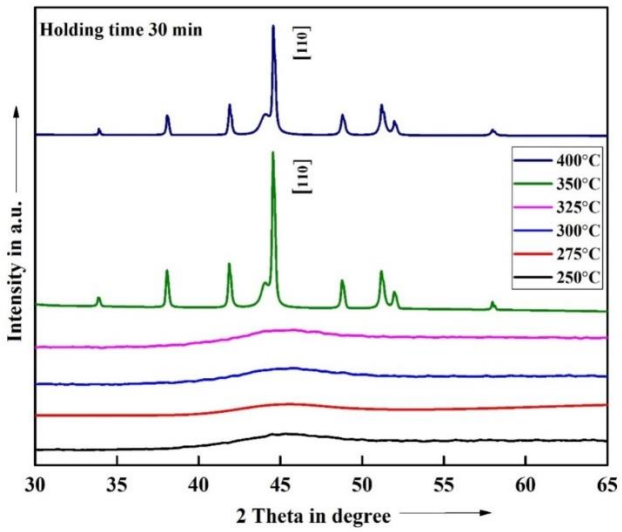

Fig. 7 XRD spectra of $Fe_{30}Ni_{50}B_{20}$ ribbon for different annealing temperatures at constant holding time 30 minutes

The lattice parameter, a_o for all the annealed samples is calculated from intense [110] diffraction peak using formula: $a_o = d_{110}\sqrt{2}$, where d_{110} is inter-planar spacing and the grain size is calculated using equation $D_g = \frac{0.9\lambda}{\beta \cos\theta}$, where the wavelength of Cu-K_α radiation λ=1.54178 Å and θ is the diffraction

angle. The calculated values of a_o, θ, FWHM (β) and D_g are shown in **Table 4** and **Table 5**. It is noticed that, with increasing annealing temperature, lattice parameter increases for short-annealed ribbon samples whereas shows random variation for 1 hour annealed samples. Pure Fe has lattice parameter of 2.8664 Å however, in the present amorphous ribbon, the lattice parameters at various annealing temperatures are significantly less than pure Fe. The diffusion phenomena in α-Fe occur during the annealing process because of the smaller atomic size of Ni as compared with Fe, the result is a contraction of lattice. Increasing trends in lattice parameters with increasing annealing temperature suggests a peak shift to staking fault as in general peak is observed experimentally.

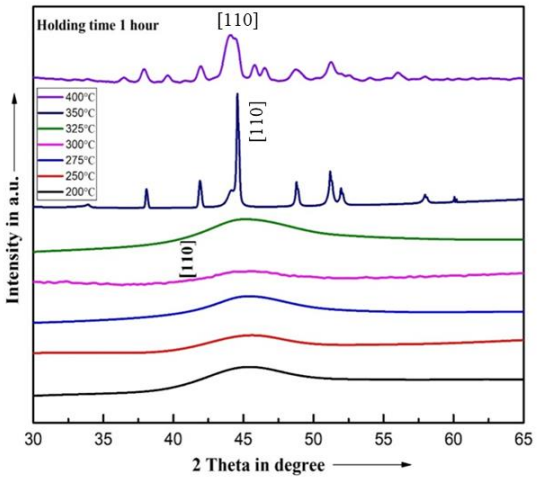

Fig. 8 XRD spectra of $Fe_{30}Ni_{50}B_{20}$ ribbon for different annealing temperatures at constant holding time 1 hour

Table 4: The experimental data estimated from XRD spectra of $Fe_{30}Ni_{50}B_{20}$ amorphous alloy annealed at different temperatures for holding time 30 minutes

Annealing temperature in °C	**Theta (deg)**	***d* (Å)**	**FWHM (deg)**	***a*o (Å)**	***D*g (nm)**	***N*i at (%)**
250	22.675	2.00901	7.5423	2.8411	2	18.22
275	22.787	2.03938	6.7575	2.8841	2	1.32
300	22.825	2.6389	5.3089	3.7319	3	386.68
325	22.905	2.7861	4.7073	3.9401	3	481.31
350	22.275	3.1312	0.5159	4.4282	29	703.18
400	22.2855	2.6417	0.6387	3.7359	24	388.5

The upper annealing temperature is limited to 350 °C and 400 °C within which grain sizes are 13 nm and 8 nm respectively for 1 hour annealing. In the annealing temperature of 350 °C and 400 °C for a short annealing time of 30 minutes grain size remains at 29 nm and 24 nm respectively to the soft magnetic α-Fe(Ni) phase. The formation of nano grain size microstructure corresponding to higher

annealing temperature is ascribed to combined effects Fe and Ni in B segregates prior growth at higher annealing temperatures of 350 °C and 400 °C.

Table 5: The experimental data estimated from XRD spectra of $Fe_{30}Ni_{50}B_{20}$ amorphous alloy annealed at different temperatures for holding time 1 hour

Annealing temperature in °C	Theta (deg)	d (Å)	FWHM (deg)	α_o (Å)	Dg (nm)	Ni at (%)
200	22.73	2.9457	8.4316	4.1658	2	583.93
250	22.7045	2.252	7.770	3.1848	2	138.00
275	22.688	2.01541	6.9665	2.8502	2	14.08
300	22.685	2.6319	5.8556	3.7220	3	382.21
325	22.5745	2.82288	4.7383	3.9921	3	504.97
350	22.2895	2.36205	1.202	3.3404	13	208.74
400	22.0475	2.1545	1.898	3.0469	8	75.32

3.3 Permeability measurement

Fig. 9 shows the frequency dependence of μ' for as-cast and different annealed samples in the temperature range 250 °C to 400 °C for a constant annealing time of 30 minutes whereas Fig. 10 shows for constant annealing time 1 hour of $Fe_{30}Ni_{50}B_{20}$ ribbon. The permeability values at different frequencies for as-cast and different annealed samples for a constant holding time of 30 minutes and 1 hour are listed in Table 6 and in Table 7 respectively.

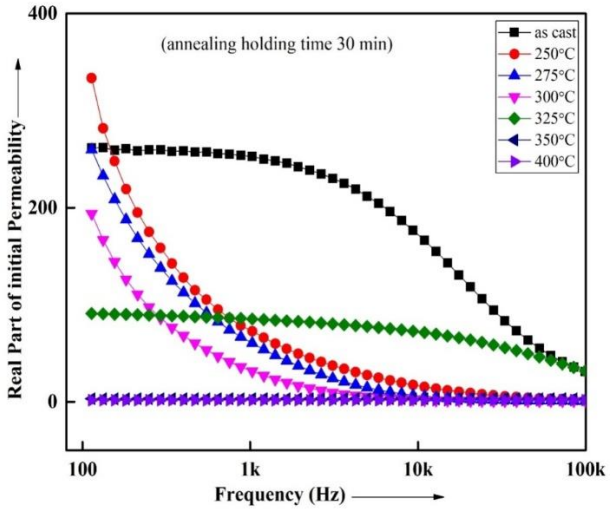

Fig. 9 Frequency dependent real permeability μ' of $Fe_{30}Ni_{50}B_{20}$ ribbon at for as-cast and different annealing temperatures at constant holding time 30 minutes

It is observed that permeability at a low frequency of 100 Hz increases and is two times greater than as-cast ribbon when annealed at 250 °C for a holding time of 1 hour. Permeability decreases with further increasing of annealing temperature and for annealing temperature higher than 325 °C initial permeability rapidly decreases and vanishes. This decrease in permeability may be attributed to the stress developed in the amorphous matrix by crystalline growth and above 350 °C the initiation of crystallization takes place as noticed from XRD spectra.

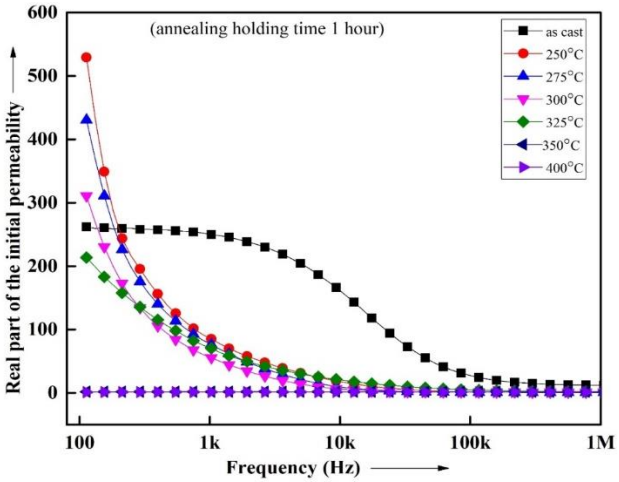

Fig. 10 Frequency dependent real permeability μ' of $Fe_{30}Ni_{50}B_{20}$ ribbon for as-cast and different annealing temperatures at constant holding time 1 hour

Table 6: The initial permeability values of $Fe_{30}Ni_{50}B_{20}$ amorphous ribbon for as-cast and annealed at different temperatures for constant holding time 30 minutes

Annealing Temperature (°C)	100 Hz	500 Hz	1 kHz	10 kHz	100 kHz
As-cast	259	256	246	118	17
250	329	112	77	17	2
275	255	97	63	16	2
300	194	56	33	3	2
325	109	88	85	72	3
350	2	2	2	2	2
400	0	0	0	0	0

Fig. 10 showed that at a low frequency of 100 Hz, the μ' is greater than the as-cast ribbon when annealed at 250 °C for holding time 30 minutes after that μ' decreases with increasing annealing temperature and permeability rapidly decreases and vanishes when annealed beyond 325 °C. The maximum value of μ'≅ 260 up to constant frequency 1 kHz for as-cast ribbon compared to the annealing temperature of 325 °C is observed μ'≅ 109 due to the stress relaxation of the amorphous matrix.

Table 7: The initial permeability values of $Fe_{30}Ni_{50}B_{20}$ amorphous ribbon for as-cast and annealed at different temperatures for constant holding time 1 hour

Annealing Temperature (°C)	100 Hz	500 Hz	1 kHz	10 kHz	100 kHz
As-cast	259	256	246	118	17
250	525	130	90	10	2
275	432	120	82	11	1
300	309	89	57	7	2
325	213	102	73	20	5
350	2	2	2	2	2
400	0	0	0	0	0

Experimentally an enhancement of permeability is observed at low frequencies up to 1 kHz range and it is also noticed that a short annealing time of 30 minutes is more effective than a long annealing time of one hour at the same annealed temperature up to 325 °C from **Table 6** and **Table 7**. These studies of two steps of 30 minutes and one hour annealing effect on permeability's provide information regarding the thermal stability of this metallic glass ribbon as transformer core at a lower constant frequency used at an elevated annealing temperature up to 325 °C. The best choice is desired in respect of two characteristics such as permeability value and its frequency dependence stable response of this metallic glass ribbon.

4. CONCLUSIONS

The crystallization behavior of the $Fe_{30}Ni_{50}B_{20}$ metallic glass ribbon based on the annealing condition as well as the initial permeability of the samples have been studied. The activation energy of the as-cast ribbon for the α-Fe(Ni) phase is 3.41 eV, whereas an annealed sample at 300 °C obtained a slightly higher activation energy of 3.91 eV for a short annealing time of 30 minutes and 3.51 eV for higher annealing time of 1 hour. For ribbons annealed at 350 °C to 400 °C and for constant higher annealing time of 1 hour, the α-Fe(Ni) phase with average grain sizes is found 8 to 13 nm but for lower annealing time of 30 minutes, average grain size is obtained 24 nm to 29 nm. The initial permeability of the metallic glass ribbon depends on the annealing temperature as well as the annealing time. The increased permeability at low frequency range annealed up to 325 °C for a higher annealing time of this metallic ribbon indicates the removal of local defects that are created during sample preparation, which facilitates domain wall movements. The drastic decrease in permeability is attributed to effective anisotropy due to the minimum grain size effect and strong magnetic coupling for higher annealing time.

ACKNOWLEDGEMENTS

The authors would like to express their thanks to Neguyen Houng Nghi, Amorphous Laboratory, Hanoi, Vietnam for the useful discussions and help in the preparation of this amorphous magnetic ribbon. The authors are thankful to the Materials Science Division, Bangladesh Atomic Energy Center, Dhaka for the measurements of XRD and gratefully acknowledge Khulna University of Engineering & Technology (KUET), Bangladesh for providing financial support for this research.

REFERENCES

[1] R. Lorentz, J. Hafiser, J. Magn. Magn. Mat., 139, 209–227 (1995).

[2] A. L. Greer, Acta Metallurgical, 30(1), 171-192 (1982).

[3] M. Zhu, M. Zhang, L. Yao, R. Nan, Z. Jian and F. E. Chang, Vacuum, 163, 368-372 (2019).

[4] L. Y. Guo, S. N. Geng, J. Pang, Y. H. Hu, S. Lan, C. M. Wang and W. M. Wang, Materials & Design, 160, 538-548 (2018).

[5] M .L. Soltani, A. Touares, T. A. Aboki and J. G. Gasser, EPJ Web of Conferences, 151, 07002 (2017).

[6] A. Said Sikder, S. D. Nath, M. N. I. Khan and S. S. Sikder, Journal of Engineering Science 13(1), 01–08 (2022).

[7] S. S. Sikder and M. A. Asgar, Thermo chimica Acta, 326, 119–126 (1999).

[8] A. Said Sikder, S. D. Nath and S. S. Sikder, Journal of Engineering Science 11(1), 107-112 (2020).

[9] M. M. Tawhid, S. K. Shil, M. T. Shihab, S. S. Sikder and M. A. Gafur, American Journal of Nano Research and Applications, 6(3), 60-66 (2018).

[10] C. D. Graham and T. Jr. Egami, Ann. Rev. Mater. Sci., 8, 423–457 (1978).

[11] S. P. Mondal, Kazi Hanium Maria, S. S. Sikder, Shamima Choudhury, D. K. Saha and M. A. Hakim, J. Mater. Sci. Technol, 28(1), 21–26 (2012).

[12] S. Brennan, R. Skomski, O. Cugat and J. M. D. Coey, Journal of magnetism and magnetic materials, 140, 971-972 (1995).

[13] K. Schnitzke, L. Schultz, J. Wecker and M. Katter, Applied physics letters, 57(26), 2853-2855 (1990).

[14] C. L. Chen and R. S. Hasegawa, J. Appl. Phys., 49(3), 1721 (1978).

[15] R. Hasegawa and R. C. O'Handley, Journal of Applied Physics, 50, 1551 (1979).

[16] H. E. Kissinger, Anal. Chem., 29(11), 1702-1706 (1957).